

## RESEARCH ARTICLE

# Reconfigurable Antenna for UAV-Assisted Wide Coverage Air-to-Ground Communications

HAKMIN LEE, YE-BON KIM<sup>1</sup>, AND HAN LIM LEE<sup>1</sup>, (Member, IEEE)

School of Electrical and Electronics Engineering, Chung-Ang University, Seoul 06974, South Korea

Corresponding author: Han Lim Lee (hanlimlee@cau.ac.kr)

This work was supported in part by the National Research Foundation of Korea (NRF) funded by the Korean Government (MSIT) under Grant 2021R1A4A2001316 and Grant NRF-2019R1A2C1088314; and in part by the Chung-Ang University Graduate Research Scholarship, in 2021.

**ABSTRACT** A wide-coverage unmanned aerial vehicle (UAV) antenna system for air-to-ground communications is proposed in this paper. The proposed antenna system has reconfigurable beam patterns based on five sets of dual-polarization and high gain antennas. Each antenna set is configured by a dual-polarization crossed inverted-V radiator and switched feed network to drive switched beamforming operations. Depending on the switch modes of the proposed antenna, main beam direction and circular polarization types can be independently selected. Further, each antenna set is faced toward the ground level at different angles from the center of UAV to provide wide beam coverage. To verify the antenna performance, each antenna set is designed at the center frequency of 5.7 GHz and total five sets are integrated with a switched feed network and a microcontroller. To implement the wide angle switched beamforming with 2-D angle-shifted main beams, a 3-D printed conformal fixture is used to connect both the antenna module and a drone body. The maximum measured bandwidth was more than 22% and the measured peak gain with the de-embedded switch feed network loss was about 10.2 dBic.

**INDEX TERMS** Dual polarization, pattern reconfigurable antenna, switched beamforming, UAV antenna, UAV communications.

## I. INTRODUCTION

The practical use of unmanned aerial vehicles (UAV) has been successfully demonstrated in various areas such as security surveillance, public safety, structural health and safety monitoring, automated inventory and agriculture applications [1], [2], [3], [4]. Also, the 3-dimensional (3-D) mobility of UAV has been prompting more intensive research for UAV-based wireless communications, aerial base station and IoT network as well [5], [6], [7], [8]. Especially, drone technology is being used widely more than ever due to its operation capability in dangerous environments, rapid relocation based on demand and improved communication coverage. Since the agility and flexibility of drone can improve line-of-sight (LoS) connections with ground users or devices, the air-to-ground communications must be thoroughly investigated. Although many different building blocks towards a successful adoption of

the air-to-ground communication-based applications such as multi-tier networks, communication channel analysis, and energy efficient transceiver can be considered, the challenges in the efficient antenna must be primarily concerned. As the high path loss from the air-to-ground should be overcome with the limited use of high power or high gain amplifier due to power consumption, high directivity antenna must be used for effective radiation. Fig. 1 (a) shows the exemplary UAV-to-ground communications, where a single drone is connected with multiple devices and users. The uniqueness of drone communications is their peak antenna LoS, which can be optimized by a tilted elevation angle due to physical locations of the communication devices. Further, to maximize the coverage of single drone to multiple devices or users, the drone antennas should cover wide range in azimuth angles as well. That is, high directivity 2-D wide-angle beamforming antenna with a tilted main beam controllability is required for the efficient drone-based air-to-ground communications. Moreover, high electromagnetic (EM) interferences due to

The associate editor coordinating the review of this manuscript and approving it for publication was Tutku Karacolak<sup>1</sup>.

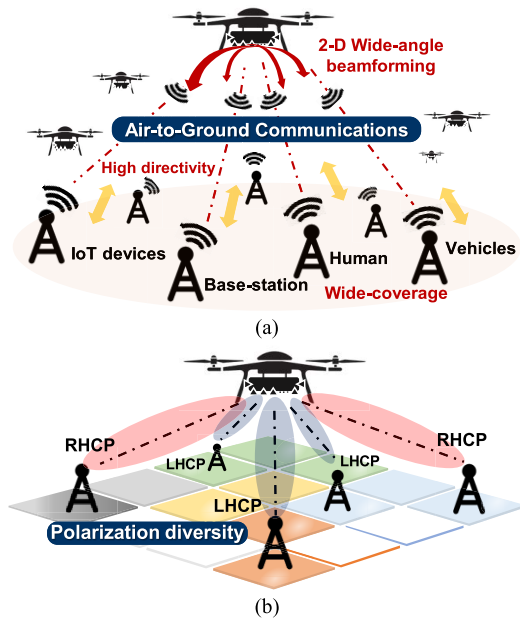


FIGURE 1. Overview of the (a) UAV-to-ground communications and (b) interference suppression by polarization diversity.

the increased number of simultaneously connected devices to a single drone must be sufficiently suppressed to avoid significant performance degradation. One of the easiest, but effective solution is the polarization diversity as shown in Fig. 1 (b). Some previously reported UAV antennas are based on conformal monopoles [9], [10] and a folded patch with metallic box [11] structures which only provide a single polarization, and thus are exposed to high EM interferences. Then, to support multiple linear polarizations (LP) for UAV or vehicular communications, SIW cavity and crossed-monopole based antennas have been proposed [12], [13]. Also, a combination of loop dipoles, circular monopole and inverted L-shaped patch antennas has been reported for 5G and V2X communications [14]. Although there are four types of polarizations such as horizontal polarization (HP), vertical polarization (VP), right-hand circular polarization (RHCP), and left-hand circular polarization (LHCP), the use of LP might be less efficient because the rapid 3-D mobility of drone complicates the LP orientation between transmitter and receiver. Also, an antenna feed network becomes more complicated if all four types of polarizations are to be used. Instead, a dual circular polarization (CP) can be considered as the efficient solution for both interference suppression and circuit complexity. Some dual-CP antennas for UAV applications or vehicular communications have been also suggested by an air-gapped patch [15], a fern-fractal-shaped microstrip [16] and a concave circular patch [17] structures. However, these antennas form broad beamwidth radiation patterns with relatively low antenna gain. Thus, they might not be suitable for the UAV applications requiring high directivity reconfigurable beam patterns. Although some reconfigurable pattern antennas with Yagi-Uda dipoles [18], half bow-tie [19], magnetic dipole [20] and planar super J-pole [21] structures have

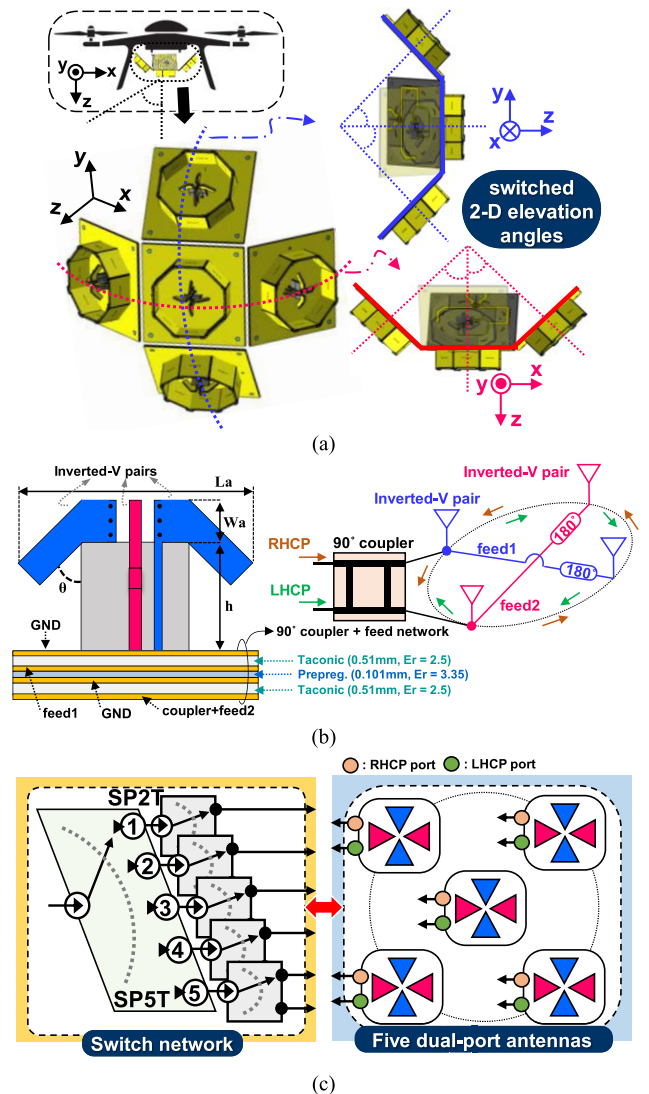


FIGURE 2. Configuration of the proposed antenna: (a) 2-D angle-shifted conformal integration, (b) a single dual-port crossed inverted-V antenna with feed network, and (c) switch network combined with five sets of dual-port antennas.

been also investigated for UAV applications, they provide LP patterns only or relatively low directivity. Therefore, to satisfy all dual-CP, high directivity and reconfigurable pattern performances, a switched-angle antenna module including both feed and control networks is proposed for UAV applications in this paper.

## II. DESIGN AND ANALYSIS OF THE PROPOSED RECONFIGURABLE ANTENNA SYSTEM

### A. SINGLE HIGH DIRECTIVITY ANTENNA DESIGN

Fig. 2 (a) shows the proposed switched-angle antenna array that can be integrated with a drone body. Since high directivity antennas generally have narrower beamwidth, multiple antennas are used to cover sufficient communication ranges for the ground devices. Total five antennas are used, and the physical center of each antenna is shifted at  $45^\circ$  in

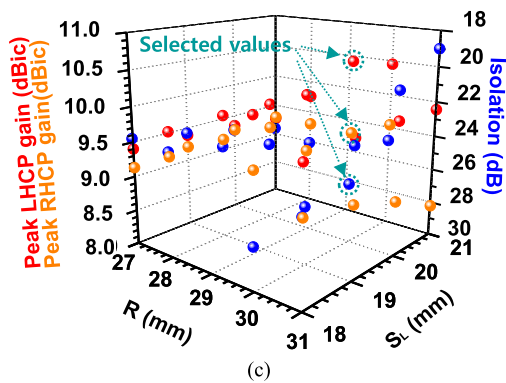
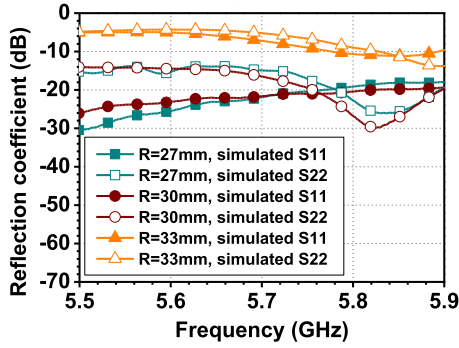
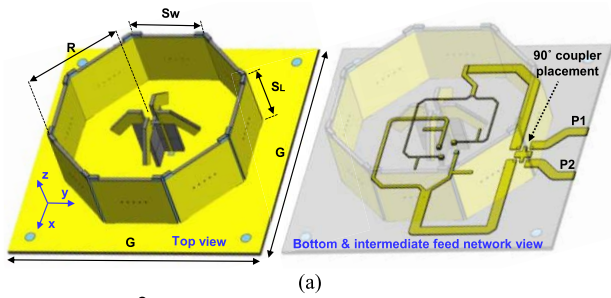


**FIGURE 3.** Gain-enhanced dual-port crossed inverted-V antenna with (a) top and bottom projection views, (b) simulated reflection coefficients according to R and (c) parameter optimization for both R and  $S_L$ .

2-D elevation angles for wide air-to-ground communication coverage. Each antenna radiation element is based on the crossed inverted-V configuration [22] with an integrated feed network configured by a single branch line coupler and four transmission lines as shown in Fig. 2 (b). By selecting the inputs of the branch line coupler, RHCP or LHCP can be generated. Thus, each antenna is designed as a dual-port antenna and connected with switch network as shown in Fig. 2 (c). The switch network is configured by a single-pole-five-throw (SP5T) switch and five single-pole-double-throw (SP2T) switches. The SP5T selects one of the five antennas with the main beam at a desired elevation angle while the SP2T selects a desired CP.

To increase the directivity of the previously reported crossed inverted-V antenna, additional ground walls surrounding each antenna are proposed in this paper. Since the fundamental analysis of the inverted-V radiator has been already discussed in [22], only the gain enhancement performance is analyzed in this section. Fig. 3 (a) shows the

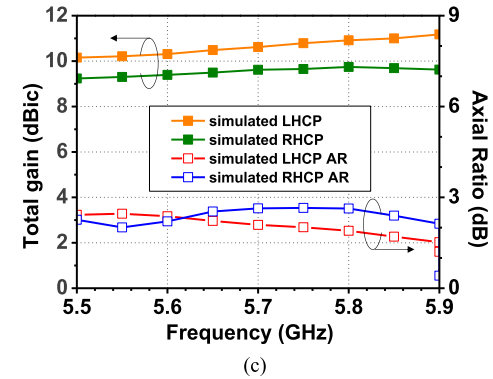
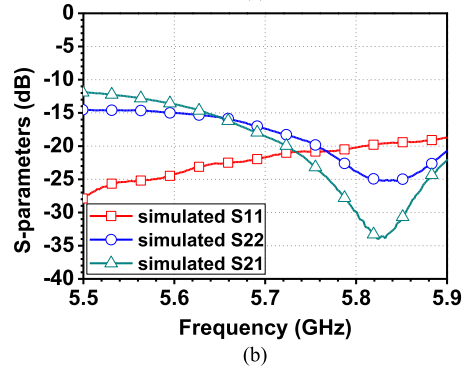
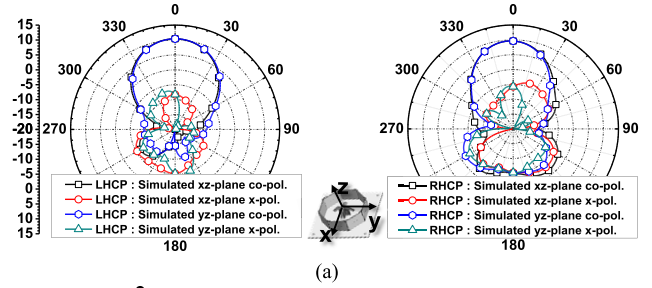


**FIGURE 4.** Proposed dual-CP antenna with simulated (a) radiation patterns at 5.7 GHz, (b) S-parameters, and (c) total gain and axial ratio within the operation band (5.5 GHz to 5.9 GHz).

proposed gain-enhanced crossed inverted-V antenna with an integrated feed network. To provide a conductive ground wall surrounding the radiator, total eight double-sided printed circuit board (PCB) pieces are used. Also, to drive both RHCP and LHCP, differential feed networks for each inverted-V pair are designed by four-layer PCB and connected with a branch-line coupler. Here, to minimize the area occupation, on-chip LTCC branch-line coupler with manufacturer-provided S-parameters is used for simulation. Then, the port 1 and port 2 represent the two inputs of the LTCC branch line coupler, and the terminals to be connected with SP2T switches. To determine the optimized parameters of the conductive wall, the reflection coefficients of the proposed antenna is first simulated by varying the radius, R, of the wall. The simulated result according to the changes in R while keeping the height of the wall,  $S_L$ , same as the height of the crossed inverted-V radiator is shown in Fig. 3 (b). Then, to further optimize both gain and isolation between two ports, parametric analysis for both R and  $S_L$  at the center frequency

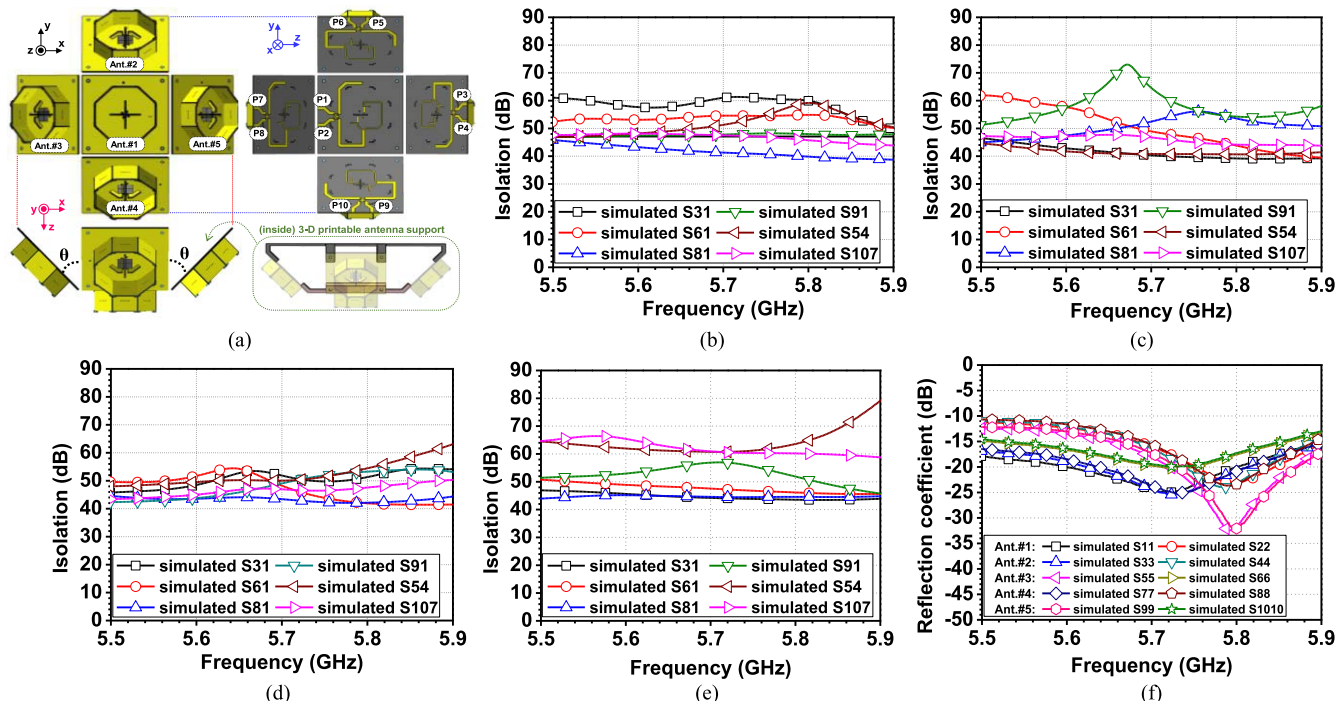


**FIGURE 5.** Proposed antenna module with (a) 3-D views, simulated isolation among each antenna set with the tilted angle ( $\theta$ ) of (b) 0, (c) 15, (d) 30, (e) 45, and (f) simulated reflection coefficients at the tilted angle of 45.

**TABLE 1.** Parameters of the proposed high gain dual-CP antenna.

Parameters	Value	Parameters	Value
$G$	84 mm	$\theta$	45°
$W_a$	5 mm	$S_L$	20 mm
$L_a$	30 mm	$S_W$	24 mm
$h$	13 mm	$R$	30 mm

of 5.7 GHz is conducted as shown in Fig. 3 (c). Based on multiple simulations, the optimized values are chosen. The determined antenna parameters are summarized as shown in Table 1.

With the selected parameters, the radiation patterns of the proposed antenna at 5.7 GHz is simulated as shown in Fig. 4 (a). The simulated peak LHCP and RHCP gains are 10.4 dBic and 9.3 dBic, respectively, resulting in more than 4 dB gain improvement comparing to the previously reported inverted-V antenna [22]. The half power beamwidths (HPBW) of LHCP and RHCP are about 50° and 46°, respectively. Also, the simulated reflection coefficients and isolation between two ports within the operation band are shown in Fig. 4 (b). Further, both simulated CP total gains and axial ratio (AR) are shown in Fig. 4 (c). The simulated gain variations in LHCP and RHCP within the operation band are less than 1.1 dB and 0.5 dB, respectively. Lastly, the simulated 3-dB AR is satisfied from 5.5 GHz to 5.9 GHz as well.

**B. SWITCHED-ANGLE UAV ANTENNA ARRAY DESIGN**

To form a switched-angle antenna array, total five sets of the gain-enhanced crossed-inverted-V are modeled as shown in

Fig. 5 (a). The center antenna of the proposed switched-angle configuration is designated for covering the area directly downward of the drone-body. The rest four antennas are tilted at an identical angle to provide main beams covering the areas with the elevation angles around the drone-body. Later, the five antennas will be integrated together by a 3-D printed antenna support and attached on the bottom of the drone-body. Fig. 5 (b)-(e) shows the simulated coupling effect across selected antenna elements from each set according to various tilted angles of the side antennas. As the tilted angle increases, the overall isolation also increases due to the increased antenna spacing. Considering both the antenna coverage and isolation characteristics, the tilted angle of 45° is chosen. Then, the reflection coefficients among the selected antenna ports from the five sets are simulated as shown in Fig. 5 (f). Since the simulated results satisfy the S-parameters within the target band, the radiation patterns of the switched-angle antenna array are simulated at 5.7 GHz as shown in Fig. 6 (a) and (b). The  $xz$  and  $yz$  planes can be referred to the 2-D elevation angles with respect to the drone-body. Fig. 6 (a) shows the simulated LHCP patterns in both  $xz$  and  $yz$  planes with each antenna’s main beam switched at 45° as desired. The maximum LHCP gain is 10.4 dBic while the gain at the overlapped patterns between two antennas is 7.3dBic. Similarly, Fig. 6 (b) shows the simulated RHCP patterns in both  $xz$  and  $yz$  planes with each antenna’s main beam switched at 45° as desired. The maximum RHCP gain is 10.1 dBic while the gain at the overlapped patterns between two antennas is 6.3 dBic. Further, the total gain and AR of LHCP and RHCP over frequencies are simulated as shown in Fig. 6 (c) and (d). The gain variations

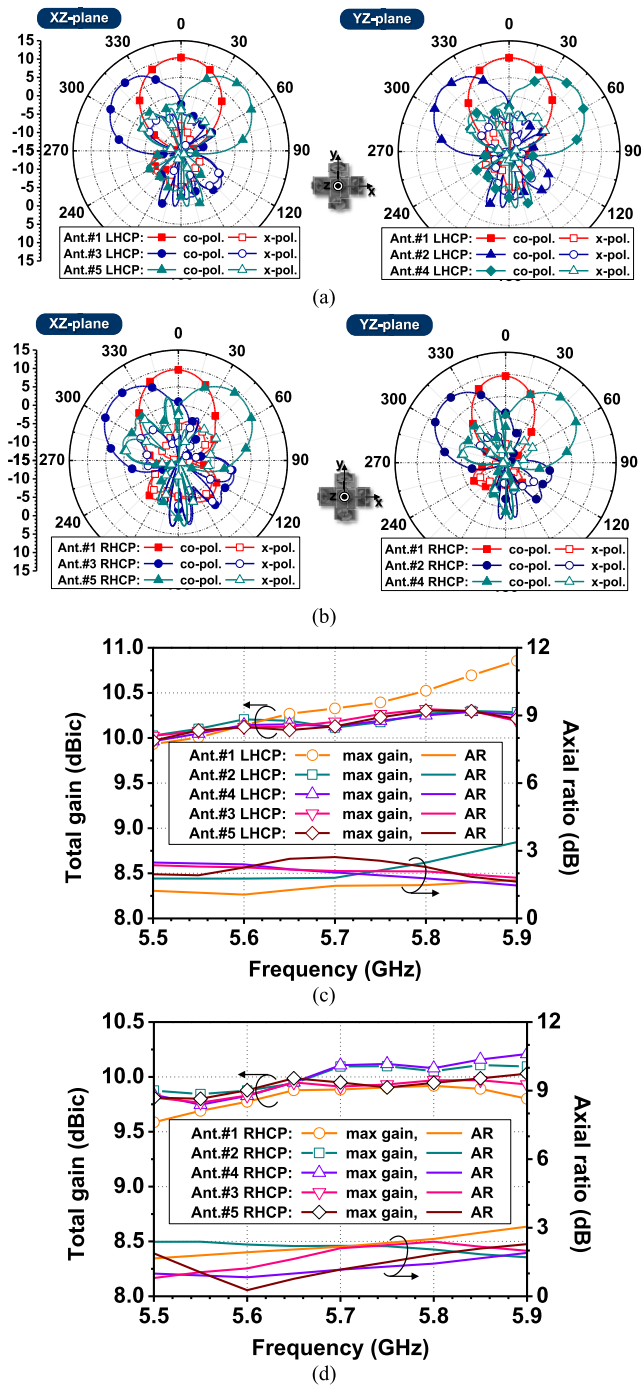


FIGURE 6. Simulated results of the proposed antenna module with (a) LHCP and (b) RHCP radiation patterns in both xz and yz planes at 5.7 GHz, and (c) LHCP and (d) RHCP total gains and AR over frequencies.

of LHCP and RHCP from 5.5 GHz to 5.9 GHz are less than 0.9 dB and 0.5 dB, respectively. Although the 3-dB AR of the proposed switched-angle antenna gets slightly degraded possibly due to the back radiation and coupling across the antenna feed network exposed on the bottom of each antenna set, the AR performance still falls into an acceptable range.

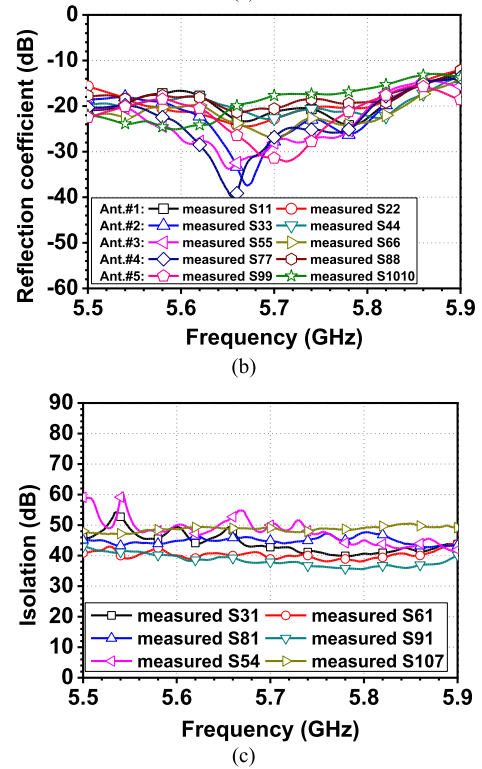
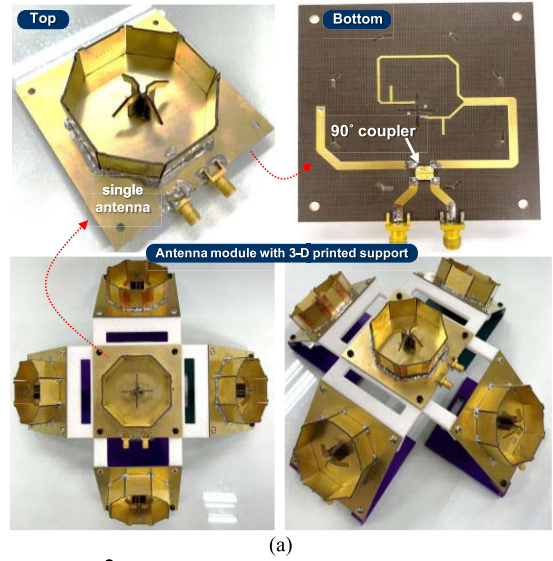
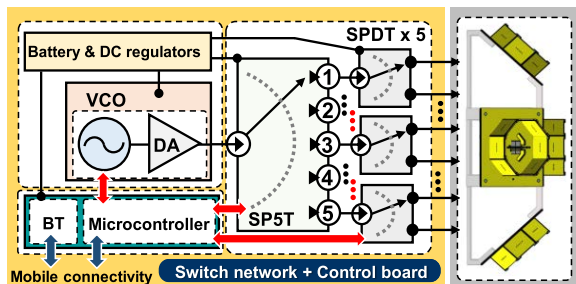


FIGURE 7. Proposed antenna module with (a) implementation, (b) measured reflection coefficients and (c) measured port-to-port isolation.

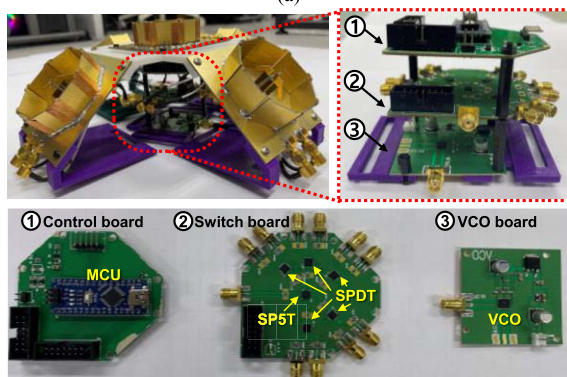
### III. FABRICATION AND MEASUREMENT

#### A. RECONFIGURABLE UAV ANTENNA ARRAY

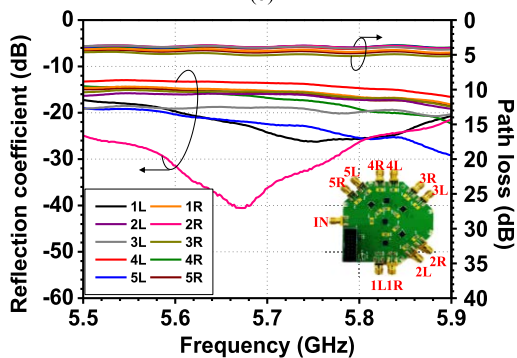
Fig. 7 (a) shows the implementation of the proposed switched-angle antenna array based on the crossed inverted-V with gain enhancement. Each antenna was fabricated with Taconic TLX-9 substrates having dielectric constant of 2.5 and loss tangent of 0.0019. The feed network was integrated by a four-layered PCB where the layer 2 and 4 (bottom) were used for each antenna pair. Here, the ground plane was



(a)



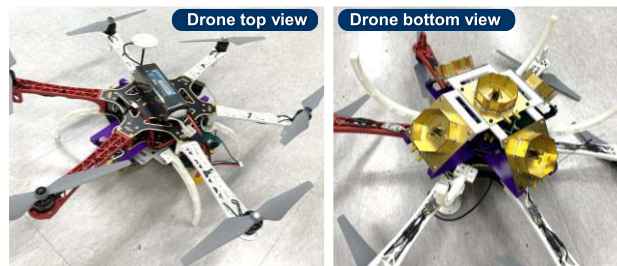
(b)



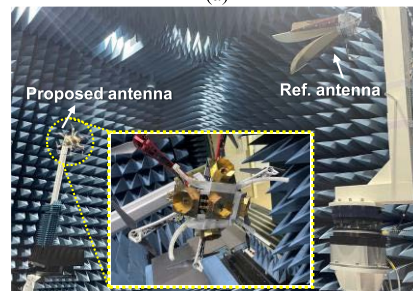
(c)

**FIGURE 8.** Control module integrated switch network: (a) overall block diagram with CW-pilot signal generator, (b) fabrication and (c) switch network measured results.

$84 \times 84 \text{ mm}^2$ , corresponding to  $1.6\lambda_0 \times 1.6 \lambda_0$  at 5.7 GHz. Also, the five antenna sets were combined together by using the 3-D printed fixture. Then, reflection coefficients and port-to-port isolation of the fabricated module were measured as shown in Fig. 7 (b) and (c), respectively. The measured 10-dB impedance bandwidth satisfied the target operation band from 5.5 GHz to 5.9 GHz. Further, the minimum isolation among the selected port from each antenna was always better than 40 dB within the operation band. Next, the complete antenna module including the switch network, control block and signal generator for field test purpose is designed as shown in Fig. 8 (a). Here, the voltage-controlled oscillator (VCO) is used to generate a pilot RF test signal at 5.7 GHz from a flying drone under test to a reference antenna on the ground. The output power of the VCO used in this paper was about 12.3 dBm at 5.7 GHz. The fabricated control,



(a)



(b)

**FIGURE 9.** Proposed antenna module with (a) drone integration and (b) radiation pattern measurement at anechoic chamber.

switch and VCO boards were stacked inside the switched angle array as shown in Fig. 8 (b). The total volume was  $265 \text{ mm} \times 265 \text{ mm} \times 100 \text{ mm}$ . The RF ports of the switch board and antennas were connected by RF cables. Moreover, the measured reflection coefficient and path losses of the switch board are shown in Fig. 8 (c). The path loss variation among each port was less than 1.1 dB while the path loss variation from 5.5 GHz to 5.9 GHz was less than 1.6 dB. Using the microcontroller unit (MCU) wirelessly connected with a mobile application through Bluetooth, the switch operations for selecting antennas and polarization types can be controlled from the ground.

To verify the radiation patterns of the complete antenna module including the drone body, the proposed antenna was integrated underneath the drone body as shown in Fig. 9 (a) and the measurement was conducted inside an anechoic chamber as shown in Fig. 9 (b). The measured radiation patterns for RHCP and LHCP in both elevation angles are shown in Fig. 10. The  $xz$ -plane was covered by the antennas 1, 3 and 5 while the  $yz$ -plane was covered by the antennas 1, 2 and 4, proving a full 2-D switched angle array performance. It is noted that the simulated results were obtained without the switch network whereas the fabricated antenna module was measured with and without the switch network. The measured maximum LHCP gain of the complete module including the switch network loss in the  $xz$ -plane was 6.6 dBic with the switched main beams at  $-50^\circ$ ,  $0^\circ$  and  $55^\circ$  as shown in Fig. 10 (a). The intermediate gains at the overlapped angles between the antennas 1 and 3, and the antennas 1 and 5 were 2.4 dBic and 2.5 dBic, respectively. The measured maximum LHCP gain of the complete module including the switch network loss in the  $yz$ -plane was 6.6 dBic with the switched

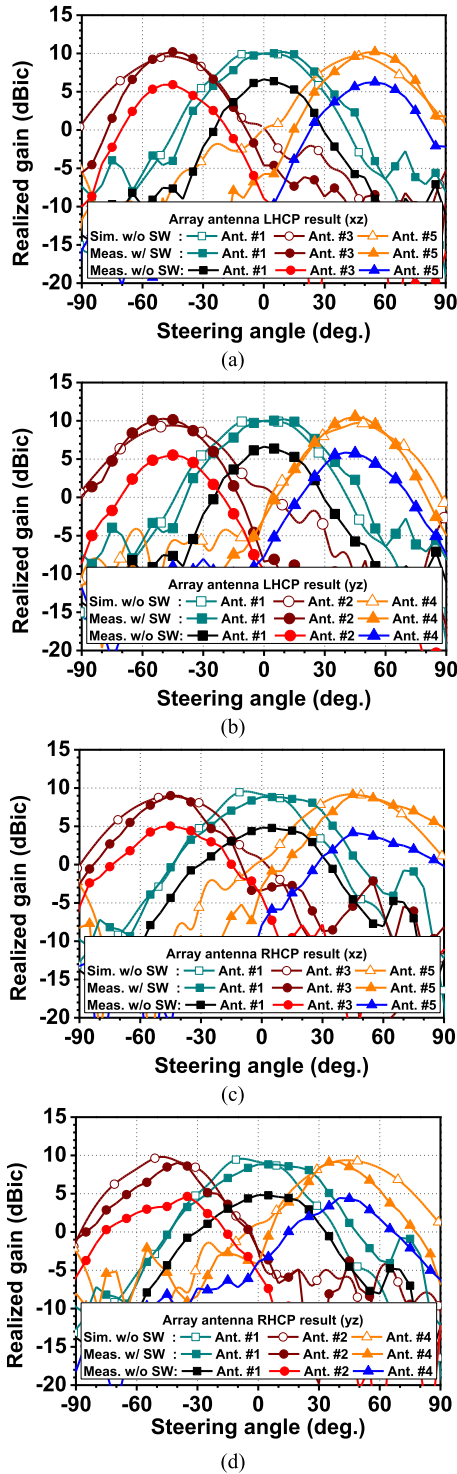


**FIGURE 10.** Measured radiation patterns for (a) LHCP in xz-plane, (b) LHCP in yz-plane, (c) RHCP in xz-plane and (d) RHCP in yz-plane at 5.7 GHz.

main beams at  $-45^\circ$ ,  $0^\circ$  and  $40^\circ$  as shown in Fig. 10 (b). The intermediate gains at the overlapped angles between the antennas 1 and 2, and the antennas 1 and 4 were 2.4 dBic and 2.6 dBic, respectively. The measured maximum RHCP gain of the complete module including the switch network

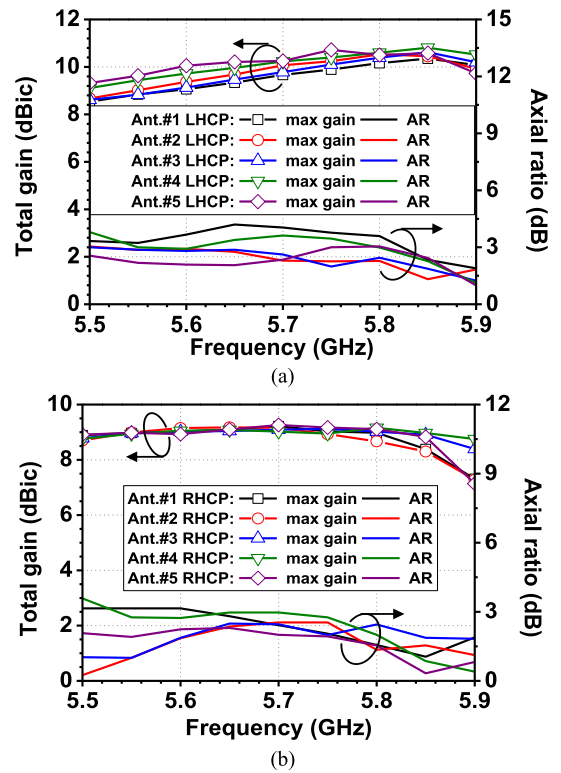


**FIGURE 11.** Measured (a) LHCP and (b) RHCP gain and AR of the proposed antenna module over frequencies.

loss in the xz-plane was 5.0 dBic with the switched main beams at  $-45^\circ$ ,  $0^\circ$  and  $45^\circ$  as shown in Fig. 10 (c). The intermediate gains at the overlapped angles between the antennas 1 and 3, and the antennas 1 and 5 were 1.1 dBic and 2.2 dBic, respectively. Also, the measured maximum RHCP gain of the complete module including the switch network loss in the yz-plane was 4.8 dBic with the switched main beams at  $-35^\circ$ ,  $0^\circ$  and  $40^\circ$  as shown in Fig. 10 (d). The intermediate gains at the overlapped angles between the antennas 1 and 2, and the antennas 1 and 4 were 2.0 dBic and 2.1 dBic, respectively. Overall, the measured and simulated gains were differed approximately by the loss of the switch network as expected. The measured peak LHCP and RHCP gains with the de-embedded switch losses were 10.2 dBic and 9.1 dBic, respectively. Further, the switched beam directions show reasonable agreement between the measured and simulated results. Next, Fig. 11 (a) shows the measured LHCP gain and AR with the de-embedded switch network loss over frequencies, where the gain variation from 5.5 to 5.9 GHz was less than 2.0 dB. Also, Fig. 11 (b) shows the measured RHCP gain and AR with the de-embedded switch network loss over frequencies, where the gain variation from 5.5 to 5.9 GHz was less than 2.1 dB. For both CP, the measured ARs were slightly degraded from the simulated results due to the effect of drone body. However, this deviation in AR can be acceptable by considering the practical measurement including the whole drone body.

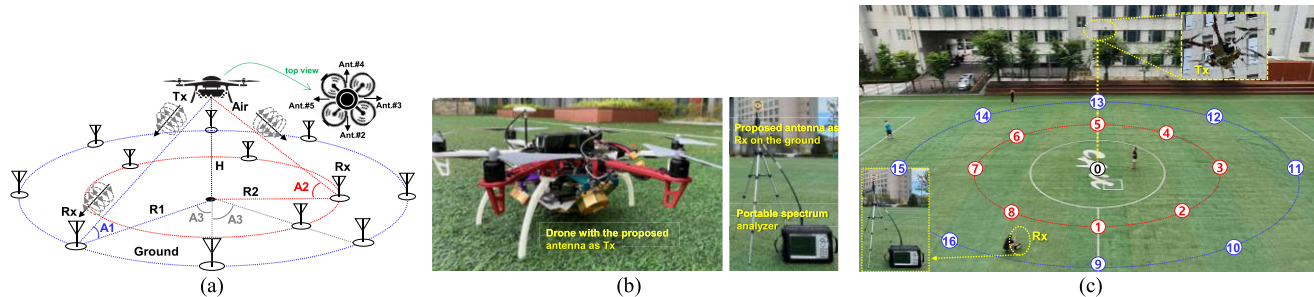


FIGURE 12. The proposed antenna integrated drone with the (a) overview of the field test, (b) antennas under test, and (c) measurement view.

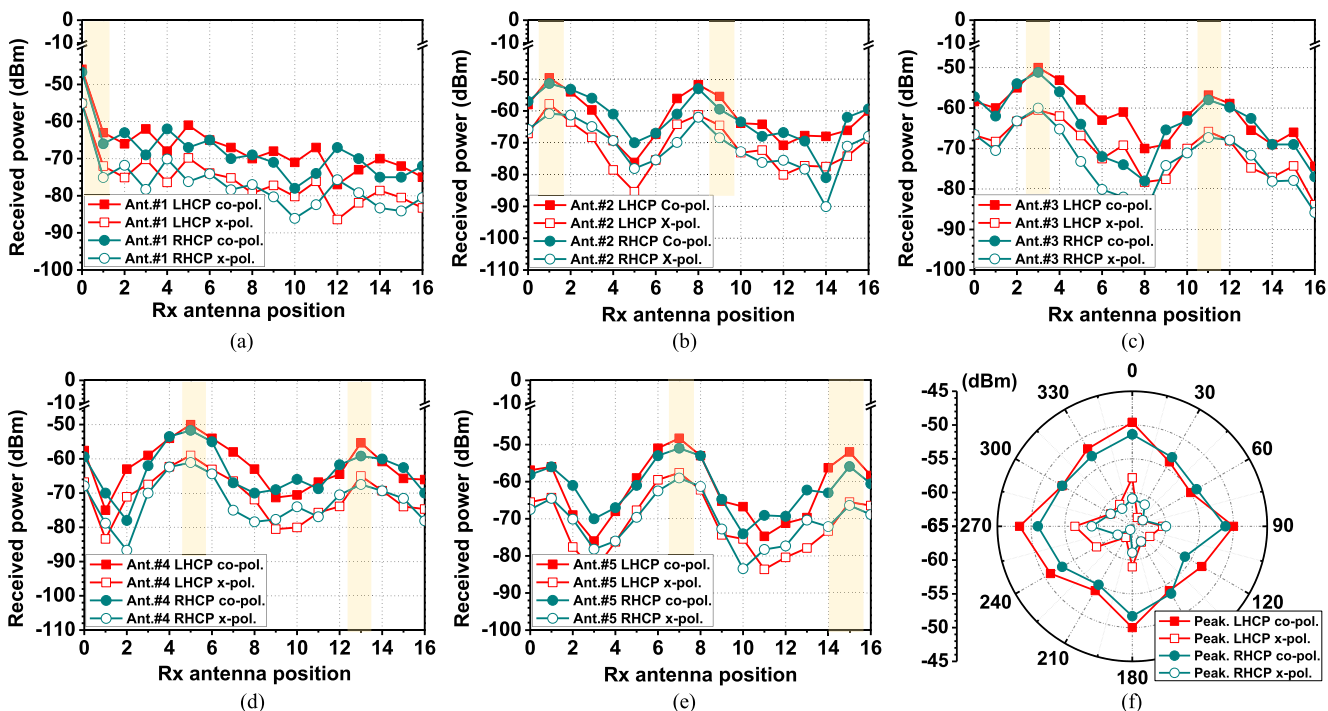


FIGURE 13. The measured air-to-ground transmission by the (a) antenna 1, (b) antenna 2, (c) antenna 3, (d) antenna 4, (e) antenna 5 with respect to Rx antenna positions, and the (f) summary of the measured azimuth channel profile.

**B. ANTENNA SYSTEM DESIGN AND AIR-TO-GROUND COMMUNICATION MEASUREMENT**

The complete antenna module integrated under the drone body was finally tested in the field as shown in Fig. 12 (a) and (b). The proposed antenna on the drone was used as a Tx sending LHCP or RHCP continuous (CW) signal from the air to LHCP or RHCP receiver antenna on the ground. The single gain-enhanced crossed inverted-V antenna with a portable spectrum analyzer was used as a Rx for both co-polarization (Tx and Rx with the same CP) and cross-polarization (Tx and Rx with the different CPs) measurement. Also, the height of the flying drone denoted by H was 5.2 m whereas the radii of Rx antenna positions R1 and R2 were 5.3 m and 7.3 m, respectively. The corresponding angles of A1 and A2 were 44.5° and 35.4° respectively. Finally, Fig. 12 (c) shows the outdoor measurement overview

where each Rx antenna position is denoted by numbers. Then, the measured co-polarization and cross-polarization of the air-to-ground transmission characteristics are presented in Fig. 13. First, Fig. 13 (a) shows the maximum received power at position 0 by the antenna 1 for both LHCP and RHCP as expected. Next, Fig. 13 (b) showed the maximum received power at position 1 by the antenna 2 as expected, but another peak was observed at position 8 instead of 9. This was due to the fabrication error that the main beam of the antenna 2 was slightly shifted in comparison to the simulated result as observed in Fig. 10 (d). According to Fig. 13 (c)-(e), the maximum received powers were observed for both LHCP and RHCP by the antennas with the desired main beam directions. Lastly, the azimuth profile according to the received power was drawn based on the switched antenna measurement as shown in Fig. 13 (f). High directivity all around the drone

with high cross-polarization discrimination (XPD) level was verified.

#### IV. CONCLUSION

In this paper, the switched-angle antenna array with high gain reconfigurable patterns and dual CP was proposed. The proposed antenna module was configured by five sets of the gain-enhanced crossed inverted V antennas, a switched feed network and MCU. The antenna radiation characteristics with the de-embedded switch feed network loss showed the measured maximum LHCP and RHCP gains of 10.2 dBic and 9.1 dBic, respectively at 5.7 GHz. Further, the switched main beams maintained high directivity for all 2-D elevation angles as well as the azimuth plane around the droned body. Moreover, the proposed antenna was fully integrated with the real drone and verified by the field test. The proposed antenna integrated drone was tested as Tx in the air while the single proposed antenna was served as Rx on the ground. The measurement for the air-to-ground transmission by the flying drone showed the excellent coverage based on the proposed switched-angle antenna operations.

#### REFERENCES

- [1] P. Wan, B. Hao, Z. Li, X. Ma, and Y. Zhao, "Accurate estimation the scanning cycle of the reconnaissance radar based on a single unmanned aerial vehicle," *IEEE Access*, vol. 5, pp. 22871–22879, 2017.
- [2] H. Baek and J. Lim, "Design of future UAV-relay tactical data link for reliable UAV control and situational awareness," *IEEE Commun. Mag.*, vol. 56, no. 10, pp. 144–150, Oct. 2018.
- [3] S. Kim, G. Lim, J. Cho, and M. J. Cote, "Drone-aided healthcare services for patients with chronic diseases in rural areas," *J. Intell. Robot. Syst.*, vol. 88, pp. 163–180, Oct. 2017.
- [4] P. D. Mitcheson, D. Boyle, G. Kkelis, D. Yates, J. Saenz, S. Aldhaher, and E. Yeatman, "Energy-autonomous sensing systems using drones," in *Proc. IEEE Sensors*, Dec. 2017, pp. 1–3.
- [5] M. M. U. Chowdhury, S. J. Maeng, E. Bulut, and I. Guvenc, "3-D trajectory optimization in UAV-assisted cellular networks considering antenna radiation pattern and backhaul constraint," *IEEE Trans. Aerosp. Electron. Syst.*, vol. 56, no. 5, pp. 3735–3750, Oct. 2020.
- [6] R. Kovalchukov, D. Moltchanov, A. Samuylov, A. Ometov, S. Andreev, Y. Koucheryavy, and K. Samouylov, "Analyzing effects of directionality and random heights in drone-based mmWave communication," *IEEE Trans. Veh. Technol.*, vol. 67, no. 10, pp. 10064–10069, Oct. 2018.
- [7] S. A. R. Naqvi, S. A. Hassan, H. Pervaiz, and Q. Ni, "Drone-aided communication as a key enabler for 5G and resilient public safety networks," *IEEE Commun. Mag.*, vol. 56, no. 1, pp. 36–42, Jan. 2018.
- [8] A. Fotouhi, M. Ding, and M. Hassan, "Flying drone base stations for macro hotspots," *IEEE Access*, vol. 6, pp. 19530–19539, 2018.
- [9] L. I. Balderas, A. Reyna, M. A. Panduro, C. Del Rio, and A. R. Gutierrez, "Low-profile conformal UWB antenna for UAV applications," *IEEE Access*, vol. 7, pp. 127486–127494, 2019.
- [10] Z.-Q. Liu, Y.-S. Zhang, Z. Qian, Z. P. Han, and W. Ni, "A novel broad beamwidth conformal antenna on unmanned aerial vehicle," *IEEE Antennas Wireless Propag. Lett.*, vol. 11, pp. 196–199, 2012.
- [11] Y. Cui, P. Luo, Q. Gong, and R. Li, "A compact tri-band horizontally polarized omnidirectional antenna for UAV applications," *IEEE Antennas Wireless Propag. Lett.*, vol. 18, no. 2, pp. 601–605, Apr. 2019.
- [12] Z. Chen, J. Tian, H. Liu, J. Yu, and X. Chen, "Novel pattern-diverse millimeter-wave antenna with broadband, high-gain, enhanced-coverage for energy-efficient unmanned aerial vehicle," *IEEE Trans. Veh. Technol.*, vol. 70, no. 5, pp. 4081–4087, May 2021.
- [13] W. Wang, Z. Zhao, Q. Sun, X. Liao, Z. Fang, K. Y. See, and Y. Zheng, "Compact quad-element vertically-polarized high-isolation wideband MIMO antenna for vehicular base station," *IEEE Trans. Veh. Technol.*, vol. 69, no. 9, pp. 10000–10008, Sep. 2020.
- [14] B. Feng, J. Chen, S. Yin, C.-Y.-D. Sim, and Z. Zhao, "A tri-polarized antenna with diverse radiation characteristics for 5G and V2X communications," *IEEE Trans. Veh. Technol.*, vol. 69, no. 9, pp. 10115–10126, Sep. 2020.
- [15] D. Wu, X. Chen, L. Yang, G. Fu, and X. Shi, "Compact and low-profile omnidirectional circularly polarized antenna with four coupling arcs for UAV applications," *IEEE Antennas Wireless Propag. Lett.*, vol. 16, pp. 2919–2922, 2017.
- [16] T. Mondal, S. Maity, R. Ghatak, and S. R. B. Chaudhuri, "Compact circularly polarized wide-beamwidth fern-fractal-shaped microstrip antenna for vehicular communication," *IEEE Trans. Veh. Technol.*, vol. 67, no. 6, pp. 5126–5134, Jun. 2018.
- [17] S. Wang, L. Zhu, G. Zhang, J. Yang, J. Wang, and W. Wu, "Dual-band dual-CP all-metal antenna with large signal coverage and high isolation over two bands for vehicular communications," *IEEE Trans. Veh. Technol.*, vol. 69, no. 1, pp. 1131–1135, Jan. 2020.
- [18] K. S. Kim, J. S. Yoo, J. W. Kim, S. Kim, J. W. Yu, and H. L. Lee, "All-around beam switched antenna with dual polarization for drone communications," *IEEE Trans. Antennas Propag.*, vol. 68, no. 6, pp. 4930–4934, Jun. 2020.
- [19] Y.-Y. Jeong and W.-S. Lee, "Wideband printed half bow-tie antenna array based on a quad-mode reconfigurable feeding network for UAV communications," *IEEE Open J. Antennas Propag.*, vol. 2, pp. 238–248, 2021.
- [20] Z. Liang, Z. Liang, Y. Li, J. Liu, J. Qin, and Y. Long, "Reconfigurable microstrip magnetic dipole antenna with switchable conical beams for aerial drone applications," *IEEE Access*, vol. 7, pp. 31043–31054, 2019.
- [21] C. Lee, G. Noh, B. Ahn, J. Yu, and H. L. Lee, "Tilted-beam switched array antenna for UAV mounted radar applications with 360° coverage," *Electronics*, vol. 8, no. 11, p. 1240, Oct. 2019.
- [22] K. Park, J. Joung, S. Lim, and H. L. Lee, "A compact crossed inverted-V antenna with a common reflector for polarization diversity in the IoT," *Electronics*, vol. 8, no. 6, p. 637, Jun. 2019.

• • •